Applied Catalysis B: Environmental 199 (2016) 504–513

Contents lists available at ScienceDirect

Applied Catalysis B: Environmental

journal homepage: www.elsevier.com/locate/apcatb

High efficiency reductive degradation of a wide range of azo dyes by SiO_2-Co core-shell nanoparticles

Yan Zhang[a], Fan Gao[a], Bridgid Wanjala[b], Zhiyang Li[a], George Cernigliaro[b], Zhiyong Gu[a,*]

[a] Department of Chemical Engineering, University of Massachusetts Lowell, One University Ave., Lowell, MA 01854, USA
[b] MicroChem Corp., 200 Flanders Road, Westborough, MA 01581, USA

ARTICLE INFO

Article history:
Received 22 March 2016
Received in revised form 31 May 2016
Accepted 9 June 2016
Available online 23 June 2016

Keywords:
Cobalt
Core-shell nanoparticles
Silica
Azo dyes
Reductive degradation

ABSTRACT

Spherical silica-cobalt (SiO_2-Co) core-shell nanoparticles were successfully fabricated for the degradation of a wide range of azo dyes. By introducing (3-Aminopropyl) triethoxysilane (APTES) to SiO_2 nanoparticle surface, which served as an amine-functional ligating agent for Cobalt (Co) reduction from Co^{2+} ions by using sodium borohydride ($NaBH_4$), size-controllable SiO_2-Co core-shell nanoparticles were synthesized. These core-shell nanoparticles were found to be highly efficient as catalysts for the degradation of a wide range of synthetic azo dyes. Methyl Orange, an example of a toxic synthetic azo dye, could be reductively degraded in aqueous solution within one minute by using 50 mg of SiO_2-Co core-shell nanoparticles at a dye concentration of 0.076 mM at pH 2.5. Kinetic studies revealed Methyl Orange degradation by SiO_2-Co core-shell nanoparticles to be first-order in reaction rate. The highest degradation rate constant k was 69.50 min^{-1} for optimized core-shell nanostructure under the above conditions. Other azo dyes, such as Orange G, Amaranth and Congo Red, processing increased complexity and more "—N=N—" double bonds, could also be reductively degraded in acidic aqueous solution by using the SiO_2-Co core-shell nanoparticles, at high reaction rates. Congo Red, due to having two "—N=N—" bonds, would need more core-shell nanoparticles in order to achieve the same amount of degradation. These SiO_2-Co core-shell nanoparticles could well play an important role as a fast treatment option, when applied to wastewater treatment.

1. Introduction

After the first synthetic dye (Mauveine) was fabricated in 1856, it is estimated that 65% −70% of dyestuff used in industry today is synthetic dye [1], of which the azo dye family (those dyes with functional "—N=N—" group) is a very important class. Compared with natural dyes, synthetic dyes have advantages of low cost, a vast range of colors, easy product coloration, and great lightfast stability. However, these properties can also cause serious environmental and health hazards [2]. As pollution of ground-water from industrial dyes and their by-products has become a serious environmental problem, a lot of attention has been focused on wastewater treatment to remove these dyes in recent years.

For the removal of dye pollutants, there are generally three treatment methods: physical, chemical and biological. Traditional physical techniques such as activated carbon adsorption [3,4], nanocomposite adsorption [5,6], ultrafiltration [7,8], ion exchange [9,10], and biological techniques such as use of bacteria, fungi, and yeasts [11–17], can degrade azo dyes. However, both physical method and biological method have limitations. For example, the resulting solid waste after physical treatment is difficult to discard; and biological treatment has strong selectivity and requires relatively harsh degradation conditions [18–21].

Chemical treatment for dye degradation, on the other hand, is considered efficient and fast [22–32]. Among different chemical treatments, use of zero-valent metals such as iron [33–36], iron-nickel alloy [37] and cobalt [2], respectively, as reductive catalysts, are showing both the effectiveness and eco-friendliness needed for efficient dye degradation. For azo dye, the azo-functional group "—N=N—" is thermodynamically favored for reductive degradation by zero-valent metal [33]. For catalyst, as is known, surface area is one of the most important factors in affecting the catalytic properties. Compared with their bulk metal counterparts, small particle size of zero-valent metal nanoparticles has the advan-

* Corresponding author.
E-mail address: Zhiyong_Gu@uml.edu (Z. Gu).

http://dx.doi.org/10.1016/j.apcatb.2016.06.030
0926-3373/

tage of high surface area, which enhances dye degradation activity [38,39]. Compared with ordinary nanoparticles of the same size, core-shell nanoparticles are easier to control, with respect to size, shape and specific function. [40] Also, they can combine the advantages of both the core and shell materials. For example, compared with pure precious material nanoparticles, an inexpensive material can be used as the core material and coated with noble or active material to reduce cost which will make core-shell nanoparticles more eco-friendly.

Silica (SiO_2) nanoparticles are considered an ideal core material, as they are inexpensive, readily available, and stable in water at elevated temperatures. [41,42] Also, SiO_2 nanoparticles can confer stability to the properties of most attached shell materials to improve nanocomposite chemical stability of the resulting colloid [43], which is critical to success in real industrial production and application. Therefore, the synthesis and use of these materials has become an active field of research due to their chemical and physical properties, as well as their potential applications.

In this paper, we used a multi-step process to synthesize SiO_2-Co core-shell nanoparticles. This synthetic method allowed us to independently control both the size of the SiO_2 core and the thickness of the cobalt shell layer. The application of SiO_2-Co core-shell nanoparticles to the degradation of a wide range of azo dyes, including Methyl Orange, Orange G, Amaranth, and Congo Red, were studied, and the reaction kinetics were investigated under several important parameters, such as initial dye concentration, catalyst dosage, and pH values.

2. Experimental

2.1. Chemicals

Anhydrous ethyl alcohol (denatured), ammonia (NH_3, 30%), tetraethyl orthosilicate (TEOS, 98%), (3-Aminopropyl) triethoxysilane (APTES, 99%), cobalt (II) chloride hexahydrate ($CoCl_2{\cdot}6H_2O$), sodium borohydride ($NaBH_4$, 99%), and sodium citrate dihydrate ($Na_3C_6H_5O_7{\cdot}2H_2O$, 99.0%), were used as purchased from Fisher Scientific. Methyl Orange (pure), Orange G (pure), Congo Red (indicator grade), Amaranth (85%, pure), and hydrochloric acid (HCl, 36.5%) were purchased from VWR Scientific. All chemicals were used without further purification. Deionized (DI) water was obtained from a Barnstead Nanopure Water Purification System.

2.2. Preparation of SiO_2 nanoparticles

Stöber's method was used to synthesize the SiO_2 nanoparticles [44]. This technique is a simple one-step process which involves the condensation and hydrolysis of TEOS in ethanol/water mixture. In a closed container at room temperature, 4 ml TEOS was well mixed with 77 ml absolute ethanol and 18 ml DI water under magnetic stirring at 1200 rpm for 10 min, following by addition of ammonia (30% NH_3). Both ammonia concentration and reaction time were varied to study their effect on SiO_2 nanoparticle size. Following reaction change from clear to opaque white, the reaction was completed and stopped at a certain time. Then, the solution was centrifuged and the isolated SiO_2 nanoparticles were washed with 3 cycles of water followed by 3 cycles of ethanol. Finally, the SiO_2 nanoparticles were re-dispersed and stored in ethanol.

2.3. Surface functionalization of SiO_2 nanoparticles

In a closed flask equipped with reflux condenser and oil bath, 0.3 g of as-synthesized SiO_2 nanoparticles (~50 nm in diameter) were reacted with APTES in 100 ml ethanol. Under stirring at 1200 rpm for 24 h at 80 °C, 0.05–25 mmol APTES (terminal amine group) was introduced onto the SiO_2 nanoparticle surface. The concentration of APTES was varied to optimize the siloxane coating on the nanoparticle surface. After reaction, the surface modified SiO_2 nanoparticles were cooled to room temperature and washed first with ethanol (3 times) followed by 3 cycles of DI water to remove residual APTES. The APTES modified SiO_2 nanoparticles were stored in DI water.

2.4. Fabrication of SiO_2-Co core-shell nanoparticles

The SiO_2-Co core-shell nanoparticles were synthesized in a closed container equipped with magnetic stirring. First, 0.08 g APTES functionalized SiO_2 nanoparticles were dispersed in 100 ml DI water. Then, cobalt chloride aqueous solution stabilized with 0.4 mM sodium citrate, was added dropwise, followed by $NaBH_4$ (0.1–0.3 g). N_2 was purged during synthesis to prevent Co oxidation. Cobalt chloride concentration was varied (1 mM–5 mM) to study its effect on Co shell structure (relative Co density in the shell layer). Scheme 1 shows both surface functionalization of SiO_2 nanoparticles by APTES and synthesis of SiO_2-Co core-shell nanoparticles.

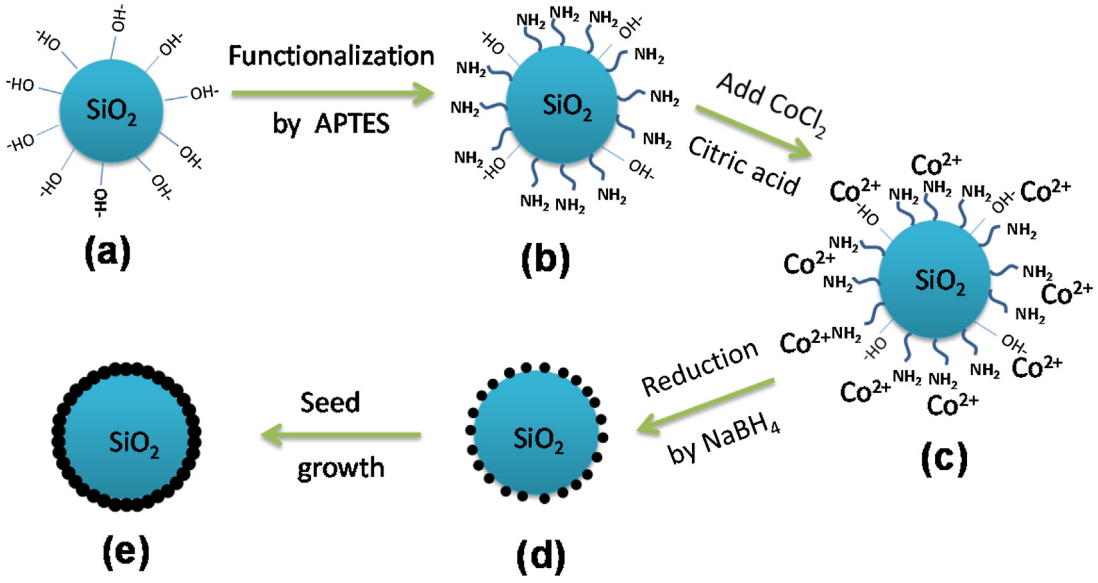

Scheme 1. Procedures for synthesizing APTES functionalized SiO_2 nanoparticles and SiO_2-Co core-shell nanoparticles.

The SiO_2-Co core-shell nanoparticles were washed with 3 cycles of centrifugation (9000 rpm/15 min) and re-dispersed in DI water to remove residual cobalt chloride. In order to protect the Co from oxidation, the core-shell nanoparticles were stored in degassed DI water under N_2 atmosphere. The freshly prepared SiO_2-Co core-shell nanoparticles were then used for azo dye degradation experiments.

2.5. Azo dye degradation by SiO_2-Co core-shell nanoparticles

Methyl Orange is a representative azo dye that has been widely used for azo dye degradation/decolorization (see Fig. S1). In this study, the SiO_2-Co core-shell nanoparticles were first used to treat Methyl Orange solutions. An aqueous solution of Methyl Orange was prepared at initial concentration of 0.076 mM (25 mg/L), and adjusted to appropriate pH values with hydrochloric acid as measured by a benchtop pH meter (model pH 510, Fisher Scientific). A 50 ml plastic tube was used as the reaction vessel. 40 ml Methyl Orange solution was first added to the tube. Then a quantified amount of SiO_2-Co core-shell nanoparticles were added to the dye solution to initiate the reaction. The core-shell nanoparticles were ultra-sonicated for 1 min before usage to facilitate better dispersion. The tube was held by the clip of a tube rotator, set at 10 rpm to prevent SiO_2-Co core-shell nanoparticles from settling during the degradation process. Samples were obtained at 0, 0.5, 1, 3, 5 and 10 min, respectively, after the reaction was initiated. After each specified time, the solid particles and liquid solutions were separated by centrifuge which took about 20 s. The liquid solution was then ready for UV/Vis measurements.

Based on the results summarized above, the SiO_2-Co core-shell nanoparticles showed rapid degradation of Methyl Orange. Three other commonly used azo dyes, Orange G, Amaranth and Congo Red, with increasing ring structure and more "—N=N—" double bonds (see Fig. S1), were chosen to further investigate the ability of the core-shell nanoparticles to treat different dyes and their degradation effectiveness, under similar reaction conditions as used for Methyl Orange.

2.6. Instrumentation

Nanoparticle imaging was performed using a JEOL JSM-7401F field emission scanning electron microscope (FESEM) operated at 10 kV and Philips EM 400 transmission electron microscopy (TEM) operated at 100 kV. TEM samples were prepared by placing a drop of nanoparticle suspension (in ethanol) on a carbon-coated copper grid, followed by drying under ambient conditions. Zeta potential measurements were performed using a Nano Particle Analyzer (Horiba SZ-100). Thermogravimetric analysis (TGA, TA-Q50) was employed to confirm the coating of APTES on surface functionalized SiO_2 nanoparticles and their relative amount. All TGA samples were dried at 150 °C in a tube furnace for 3 h under N_2 reflow, before analysis, and the measurements were performed in the temperature range of 20–800 °C under nitrogen atmosphere, with a heating rate of 20 °C min^{-1}. UV/Vis absorption spectra were obtained using a Perkin Elmer Lambda 25 spectrophotometer to determine the concentrations of azo dyes and possible degradation products within the wavelength range of 200 nm–750 nm.

3. Results and discussion

3.1. SiO_2 nanoparticle synthesis

The size of SiO_2 nanoparticles varied when changing the molar ratios between ammonia, ethanol and water to TEOS. In this work, the effect of ammonia concentration and reaction time on SiO_2 nanoparticle synthesis was studied and optimized in order to obtain a viable core-shell nanostructure with good catalytic property toward azo dye degradation.

3.1.1. Effect of ammonia concentration

Ammonia, which catalyzes TEOS hydrolysis and condensation, plays an important role in regulating SiO_2 nanoparticle size. In this study, the ammonia concentration was varied in conjunction with fixed quantities of water, ethanol, TEOS and reaction time. From the SEM and inset TEM images as shown in Fig. 1, SiO_2 nanoparticles grew larger with increasing ammonia concentration from 150 mM to 250 mM over the same reaction period of 160 min. The mean particle sizes were measured from TEM images, varying from 30 ± 3.7 nm to 94 ± 15.4 nm, as summarized in Fig. 1(d).

In addition, by increasing ammonia concentration, the yield of corresponding SiO_2 nanoparticles also increased from 6% to 50%. Our results compare well with other referenced work [45], which indicated that when NH_3 concentration is relatively low such as 100 mM, either longer reaction time is required, or SiO_2 nanoparticles do not form. In contrast, when NH_3 concentration is 250 mM, there is a risk of coagulation and nanoparticle size distribution becoming larger, as shown in Fig. 1(d). Thus, the ammonia concentration was fixed at 200 mM for the following experiments, with an average particle size around 50 nm.

3.1.2. Effect of reaction time

Reaction time is yet another factor that can affect SiO_2 nanoparticle size during synthesis, where the size was observed to increase with increasing reaction time. The effect of reaction time on SiO_2 nanoparticle size, employing the chosen ammonia catalyst concentration of 200 mM, is shown in Fig. S2 (see Supplementary Material), which indicates an almost linear relationship between the nanoparticle size and reaction time. Since SiO_2 nanoparticle synthesis involves TEOS hydrolysis in ethanol medium in the presence of ammonia, increase in reaction time provides opportunity for SiO_2 seeds to grow, which leads to larger SiO_2 nanoparticles.

Ultimately, both ammonia concentration and reaction time affected the final SiO_2 nanoparticle size formed. Based on the results above, 200 mM was chosen as the ammonia concentration, with 160 min as the reaction time, to produce ~0.3 g of SiO_2 nanoparticles with approximately 50 nm in diameter. The selection of this size is to ensure that the final core-shell nanoparticles are smaller than 100 nm.

3.2. Surface functionalization of SiO_2 nanoparticles

The purposes of APTES surface functionalization are to (1) increase the efficiency of reduced cobalt to attach to the SiO_2 core, and (2) ensure the location of subsequently reduced cobalt sites, such that the outcome is a homogeneous cobalt seed surface and, after further cobalt reduction and surface attachment, a homogeneous cobalt shell, all as represented in Scheme 1(a–e).

In this process, the stability of dispersed SiO_2 nanospheres in aqueous media (Scheme 1a) derives from negatively charged SiO_2 surface resulting from full deprotonation of surface silanol. After APTES functionalization (Scheme 1b), the effect of surface negative charge is somewhat muted, due to increasing positive charge resulting from amine protonation, which occurs during APTES functionalization. This surface charge correlates to the zeta potential values (see Fig. 2), and can be explained by noting that, although APTES surface modification may not be 100% achieved, there is still enough loss in net negative surface charge to impact ligation of cobalt ion or cobalt seeding to SiO_2 surface.

The uniform APTES surface modification layer helped the cobalt seeding process to the surface of SiO_2 nanoparticles to form uniform cobalt shell. Fig. 2(a) shows the effect of APTES concentration (0.5 mM–250 mM) on the size of SiO_2 core nanoparticles. The

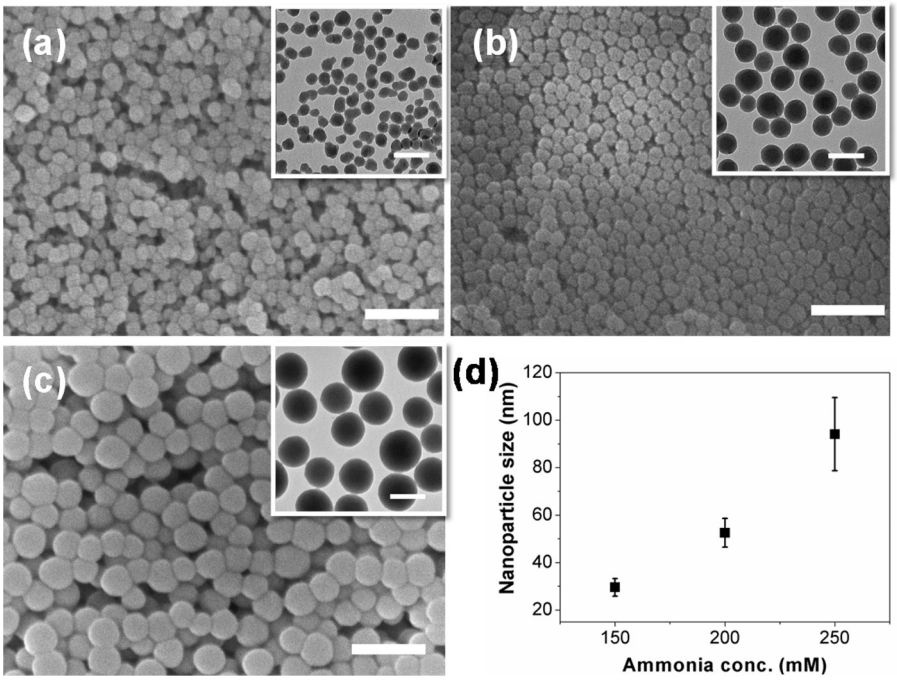

Fig. 1. Images showing the effect of ammonia concentration on the size of SiO_2 nanoparticles at constant reaction time of 160 min, (a) 150 mM ammonia; (b) 200 mM ammonia and (c) 250 mM ammonia, respectively (Scale bar for SEM images is 200 nm and scale bar for inset TEM images is 100 nm); (d) A summary of size analysis with increasing ammonia concentration.

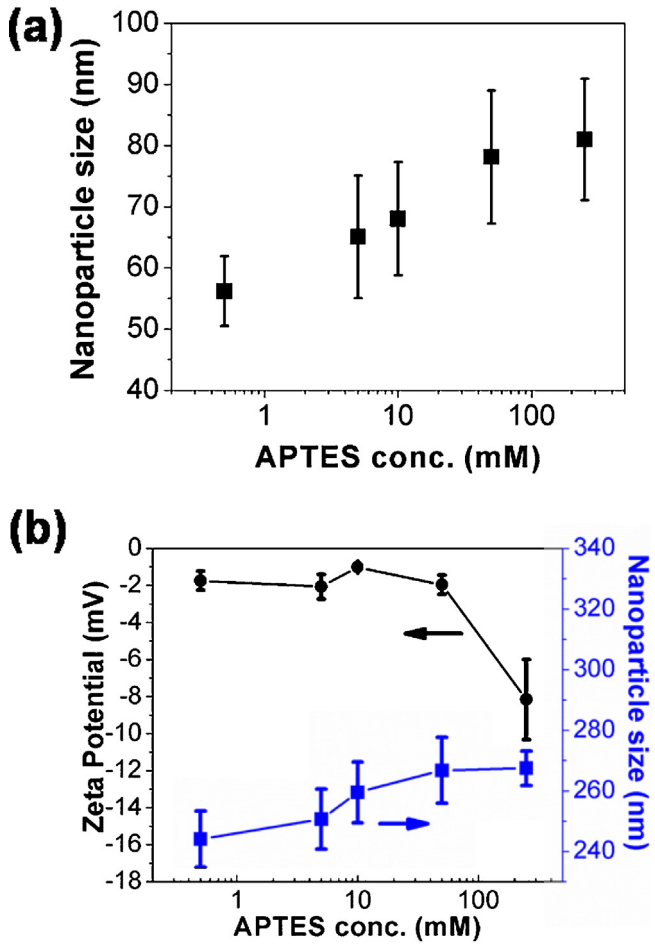

Fig. 2. Effect of APTES concentration on functionalized SiO_2 nanoparticles. (a) Size analysis based on TEM images; (b) Zeta potential and size measurement by DLS.

size of functionalized SiO_2 core increases with increasing APTES concentration, but levels off between 50 mM and 250 mM. After functionalization, the size of SiO_2 nanoparticles grew from approximately 56 nm to 81 nm, which indicated that the increased size was due to APTES hydrolysis during the reaction.

The zeta potential of the non-functionalized SiO_2 nanoparticles was measured to be −120 mV, which means that they were easily dispersed and very stable in the aqueous solution. The surface modification of the SiO_2 nanoparticles with APTES significantly increased the zeta potential value to be closer to zero, as shown in Fig. 2(b). With a small amount addition of APTES (0.5 mM), the zeta potential of the SiO_2 nanoparticle solution quickly increased to almost zero (∼−1 mV), indicating less stability. This is consistent with our observation that, after surface functionalization of the SiO_2 nanoparticles, the APTES modified SiO_2 nanoparticles tend to aggregate and precipitate more easily in the aqueous solution. However, when the APTES concentration increased from 0.5 mM to 250 mM, the Zeta potential of the APTES functionalized SiO_2 nanoparticles changed from −1 mV to −8 mV, indicating slight increase in stability. At the same time, the size of the APTES functionalized SiO_2 nanoparticles measured by dynamic light scattering (DLS) increased slightly from 244 nm to 268 nm, an increase of 10%, as shown in Fig. 2(b). When the sizes measured from DLS are compared to the nanoparticle sizes measured from TEM images as shown in Fig. 2(a), the aggregation state of the particles can be determined. The hydrodynamic diameter from DLS is typically 3–5 times larger than the particle size from the TEM measurements, indicating slight aggregation. Further analysis shows that, the 10% increase of the sizes measured by DLS is much lower than the 45% increase from TEM measurement, from 56 nm to 81 nm when the APTES concentration increased from 0.5 mM to 250 mM; this indicates a decrease of nanoparticle agglomeration, which is consistent with the increased stability of APTES functionalized SiO_2 nanoparticle from zeta potential measurements in the APTES concentration range studied.

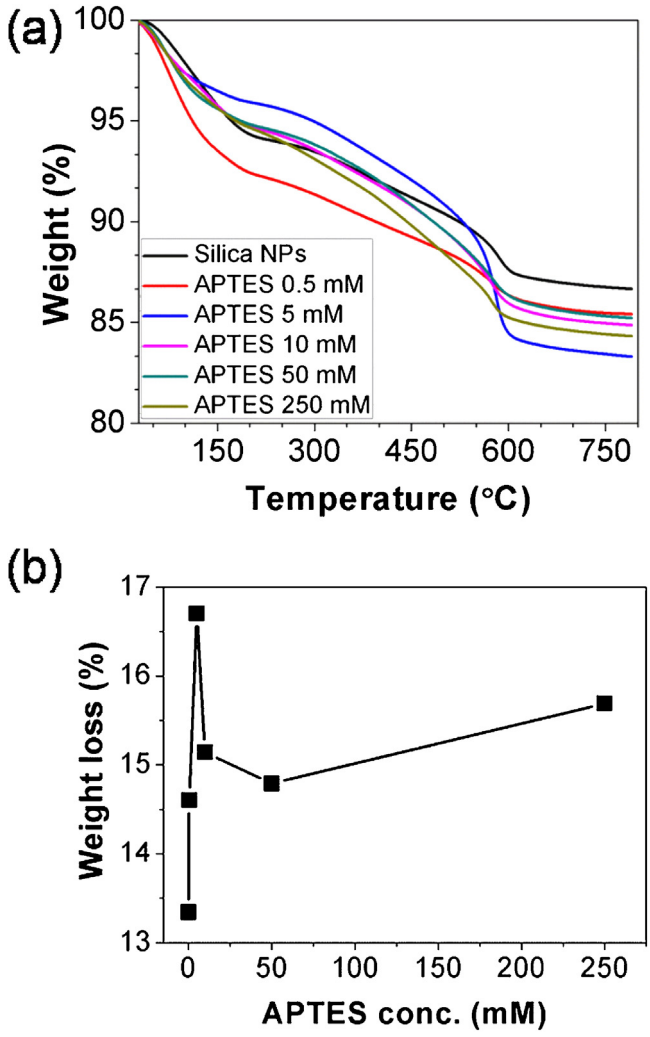

Fig. 3. (a) Thermogravimetric analysis (TGA) curves of SiO_2 nanoparticles before and after surface functionalization using different concentrations of APTES; (b) A plot of weight loss of functionalized SiO_2 nanoparticles versus concentration of APTES that was used for surface functionalization.

The efficiency of surface functionalization by APTES was also evaluated by TGA measurements, as shown in Fig. 3. Typically, the desorption of physisorbed water is completed at 150 °C and followed by a broad region of weight loss which is usually completed at 180 °C, due to the dehydroxylation process [46]. In our experiments, all the samples were dried before TGA test, in order to remove moisture in samples. However, the APTES modified SiO_2 nanoparticles still showed 4% weight loss, attributed to moisture and possibly due to water molecules reattachment to the sample during a short time sample transfer process before the measurement. Weight loss between 180 °C–600 °C was attributed to loss of APTES, while weight loss above 600 °C was attributed to the fritting of SiO_2 [47]. As shown in Fig. 3(a), the different functionalized SiO_2 nanoparticles (by varying concentrations of APTES) showed different weight loss, which indicates the concentration of APTES would affect the efficiency of surface functionalization. [48]

From Fig. 3(b), the weight loss for pure SiO_2 nanoparticles is 13.3%, which is close to the weight loss of low concentration (0.5 mM) APTES surface modification (14.6%), indicating that low APTES concentration does not produce good functionalization. However, by increasing APTES concentration to 5 mM, 16.7% of bulk weight was lost. This was caused by loss of the organic long chain structure of APTES. With increasing APTES concentration, less weight is lost. For example, 15.1% for 10 mM APTES, 14.8% for 50 mM, and 15.7% for 250 mM, which may indicate that the quality of the surface modification is not correlated with increasing APTES concentration above 10 mM, where loss seems to level off. Based on the results above, 5 mM APTES was used for maximizing the surface modification of the SiO_2 nanoparticles. Weight loss for pure SiO_2 nanoparticles was caused by a dehydroxylation process, whereby hydroxyl group coupling on SiO_2 surface forms H_2O, which subsequently evaporates (dehydration). From L.T. Zhuravlev's review, desorption of physisorbed water was completed at 150 °C and was followed by a broad region of weight loss, due to dehydroxylation process [46]. For APTES functionalized SiO_2 nanoparticles, hydroxyl group on SiO_2 surface were replaced by organic chain. Weight loss occurring between 180 °C and 600 °C was attributed to a decarbonization process, whereby organic chain (APTES) was burned-off to become CO_2.

3.3. SiO_2-Co core-shell nanoparticles

$CoCl_2$ aqueous solution (Co^{2+}) was added to the surface modified SiO_2 nanoparticles [Scheme 1(b)] at room temperature. In order to ensure full reduction of Co^{2+} ions to Co nanoparticles, a strong reducing agent $NaBH_4$ was utilized. Co^{2+} initially formed small Co seeds which attached to SiO_2 surface, such that the outcome was a homogeneous cobalt seed surface. After further cobalt reduction and surface attachment, Co seeds grew to large Co nanoparticles, thus forming a shell layer on the SiO_2 nanoparticles. Ultimately, well dispersed SiO_2-Co core-shell composite nanoparticles were obtained (see Fig. 4). The formation of Co nanoparticles during the $NaBH_4$ reduction process was confirmed by the dramatic color change of the solution after introduction of the reducing agent. Further characterization by magnetic separation also confirmed the formation of Co nanoparticles due to the magnetic property of the Co (see Fig. S3).

The overall reaction proposed for this core-shell formation process is, [49–51]

$$2Co^{2+} + BH_4^- + 2H_2O \rightarrow 2Co(s) + 2H_2(g) + 4H^+ + BO_2^- \quad (1)$$

The release of hydrogen gas (H_2), as shown in the above equation, is believed to help protect cobalt particles from oxidation during the reaction process.

The concentration of Co^{2+} ions in the precursor solutions would significantly affect the surface of the SiO_2-Co core-shell nanoparticles. Fig. 4 provides the TEM images of the SiO_2-Co core-shell nanoparticles with different structures (structure 1–4, abbreviated as CS-1 to CS-4 below) in each growth stage. With initial Co^{2+} concentration of 1 mM (corresponding to CS-1) and 2 mM (CS-2), as shown in Fig. 4(a) and (b), some dot structure formed and grew on the surface of SiO_2 core, which indicates reduction of Co^{2+} ions to metallic Co atoms and the nucleation of Co. When the Co^{2+} concentration was increased to 2.5 mM (CS-3), the reduced Co seemed to be saturated on the nanoparticle surface and started to form some bridging between some SiO_2 nanoparticles (Fig. 4(c)), indicating excess Co nanoparticle formation after saturation. When the concentration was increased to 5 mM (CS-4), the reduced Co formed a sheet-like, rough and textured structure on SiO_2 surfaces, as shown in Fig. 4(d). This evolution of Co coating structures is shown in Scheme 1. The Co seeds first attach to SiO_2 surface and then grow to larger Co nanoparticles, and finally form sheet-like Co shell surrounding the SiO_2 nanoparticles. Higher magnification TEM image analysis of the sheet structures (Fig. S4) in the samples CS-3 and CS-4 indicated that the sheet layers connecting different SiO_2 nanoparticles are composed of many small Co nanoparticles, which added more Co contents and can further improve the catalytic ability of these core-shell structures.

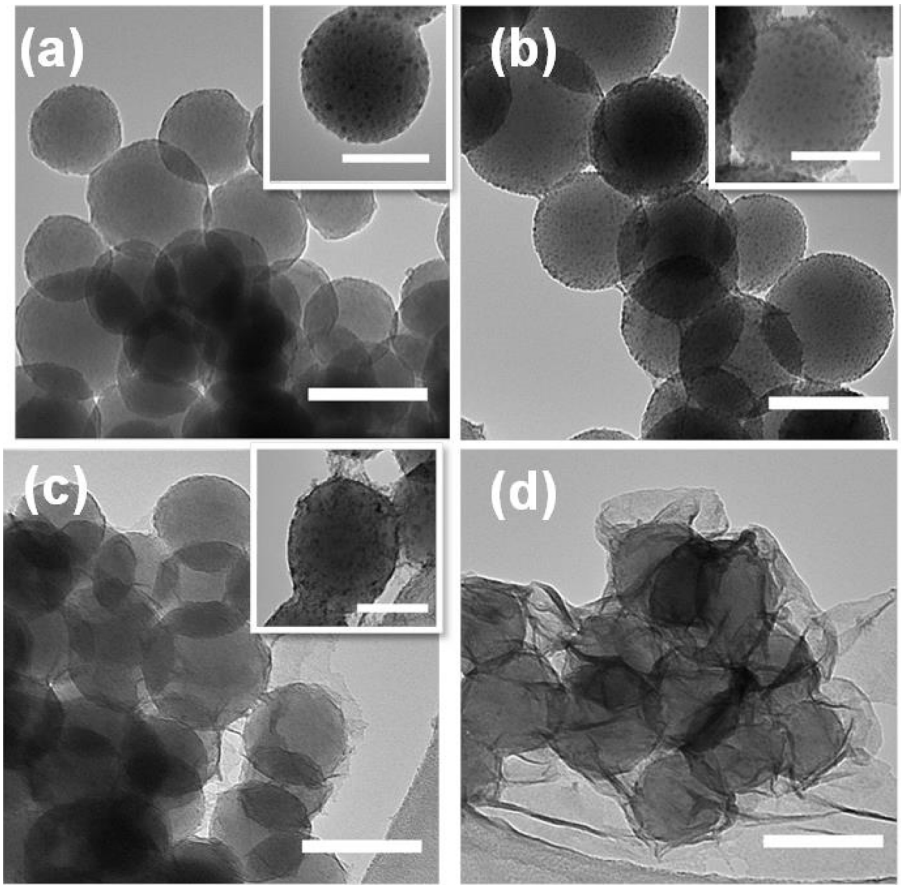

Fig. 4. TEM images of SiO_2-Co core-shell nanoparticles synthesized with various Co^{2+} precursor concentrations (Scale bar 100 nm; inset scale bar 50 nm); (a) CS-1 (prepared from 1 mM Co^{2+} precursor solution); (b) CS-2 (from 2 mM Co^{2+}); (c) CS-3 (from 2.5 mM Co^{2+}); (d) CS-4 (from 5 mM Co^{2+}).

Reaction for SiO_2 core surface functionalization is very robust and reproducible, thus providing a reliable monolayer of surface functional groups. As this monolayer may not be visible by SEM and TEM imaging, EDX was used to detect and quantify the elemental composition of the samples at every stage. CS-3 sample was used to represent SiO_2-Co core-shell nanoparticles for EDX analysis. In order to avoid the overlap effect of silicon substrate, all samples were prepared on carbon tapes. As shown in Fig. 5, for all three samples (SiO_2 nanoparticles, APTES functionalized SiO_2 nanoparticles, and SiO_2-Co core-shell nanoparticles), the main elements are silicon and oxygen. The difference in EDX response between SiO_2 core and APTES-functionalized SiO_2 is that, after functionalization, the spectrum shows more carbon, resulting from the APTES hydrocarbon chain. In further contrast, SiO_2-Co core-shell nanoparticles show the obvious cobalt peak and no obvious peak for carbon, indicating that the cobalt layer is deposited directly onto the functionalized SiO_2 core.

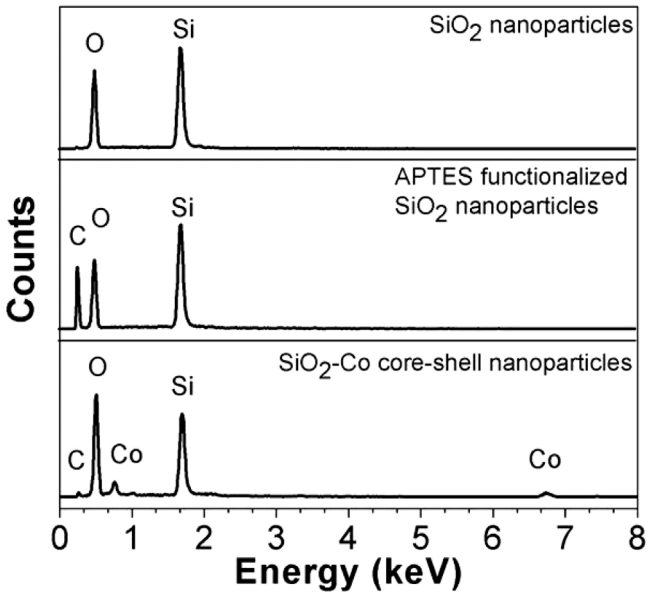

Fig. 5. EDX analysis of SiO_2 nanoparticles, APTES functionalized SiO_2 nanoparticles, and SiO_2-Co core-shell nanoparticles.

3.4. *Methyl orange degradation by SiO_2-Co core-shell nanoparticles*

For azo dyes, including Methyl Orange, the double bond ("—N=N—") is the characteristic and chromophoric group for color. [2,52] The SiO_2-Co core-shell nanoparticles were first used to treat Methyl Orange dye solution, as the dye molecule possesses only one azo-functional group (—N=N—) and is the simplest model azo dye. UV/Vis spectroscopy was the primary tool used for determination of Methyl Orange concentration in aqueous solution. The initial pH of 2.5 for Methyl Orange indicates a moderately strong acid. Fig. 6(a) shows the variation of UV/Vis absorbance spectra as a function of nanoparticle treatment time; the main absorption peak for Methyl Orange occurs at 506 nm [53] and this peak decreased quickly during reaction. Also, following addition of SiO_2-Co core-shell nanoparticles to Methyl Orange aqueous solution (initial dye

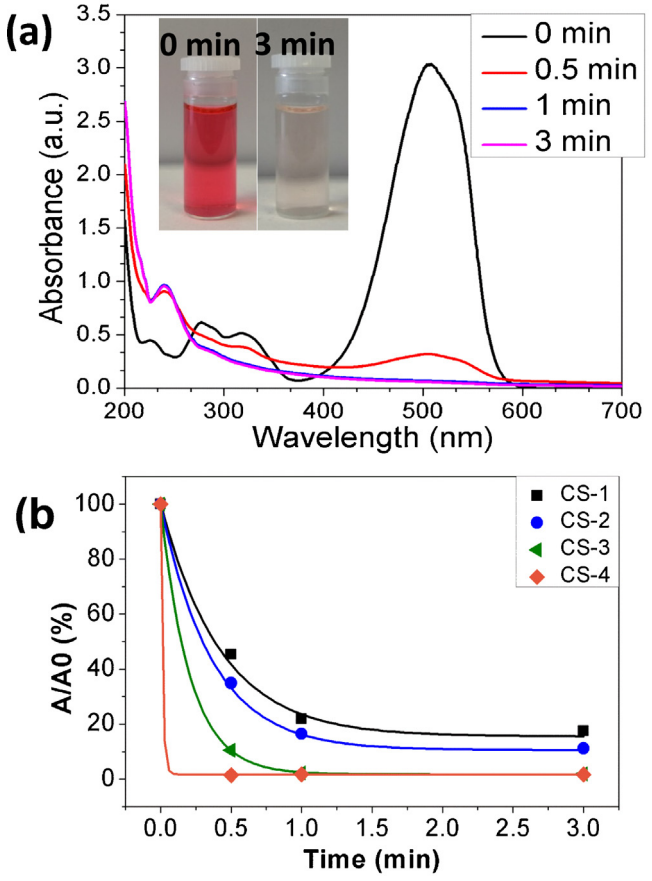

Fig. 6. Methyl Orange degradation by SiO_2-Co core-shell nanoparticles at pH 2.5 with an initial Methyl Orange concentration of 25 mg/L; (a) UV/Vis absorption spectra (inset optical images of dye before & after treatment); (b) The surface structure effect on degradation kinetics. (For interpretation of the references to colour in the text, the reader is referred to the web version of this article.)

concentration 0.076 mM, or 25 mg/L), solution color changed from an initial red to colorless within 1 min, as shown in Fig. 6(a).

A new UV/Vis absorbance peak, which formed concurrently at wavelength 243 nm during dye treatment, can be explained as resulting from cleavage of the azo bond ("—N═N—") and formation of new degradation products. It is believed that the degradation of Methyl Orange by the SiO_2-Co core-shell nanoparticles is similar to the results from hollow Co nanoparticles from Sha et al. [2], and possible degradation products include sulfanilic acid and *N*, *N*-Dimethyl-*p*-phenylenediamine, which have UV absorption at wavelength 248 nm [54] and 242 nm [2], respectively. This indicates that the SiO_2-Co core-shell nanoparticles reductively decomposed Methyl Orange in aqueous solution, instead of pure adsorption. This new absorbance peak was observed in all the core-shell nanoparticles, as shown in Fig. S5.

Fig. S5 showed Methyl Orange degradation by 80 mg of four different SiO_2-Co core-shell nanoparticles, respectively, when added into 40 ml Methyl Orange aqueous solution with the same initial dye concentration. Kinetic curves (Fig. 6(b)) showed that high Co concentration structures (CS-3 and CS-4) degraded Methyl Orange faster and more efficiently than low Co concentration structures (CS-1 and CS-2). Furthermore, the final degradation amounts from structures CS-3 and CS-4 almost overlapped, indicating that both CS-3 and CS-4 have enough Co nanoparticles on their surfaces to treat Methyl Orange dyes. The results above indicate that Co shell structure was a main factor for Methyl Orange degradation rate.

As the kinetic results shown in Fig. 6(b), even though the same amount of SiO_2-Co core-shell nanoparticles (80 mg) was used for

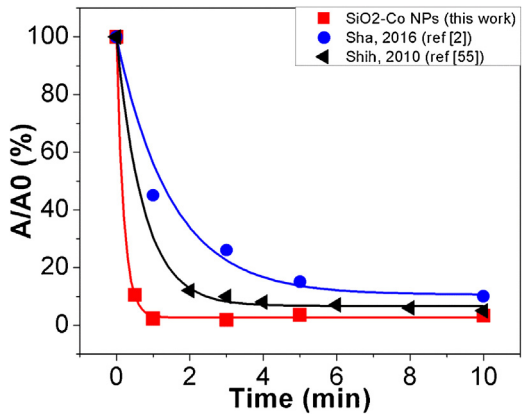

Fig. 7. Comparison of Methyl Orange degradation at pH 3 by SiO_2-Co core-shell nanoparticles with Sha's and Shih's work.

the experiments, complete degradation was not achieved with core-shell nanoparticles CS-1 and CS-2. On the other hand, over 99% degradation was achieved with core-shell nanoparticles CS-3 and CS-4 after 1 min. Since CS-3 used less Co salt in the precursor solution (only half of the amount compared to CS-4), it was selected to be used in the following azo dye degradation experiments. Corresponding UV/Vis spectra and optical images of the dye degradation are shown in Fig. S5. Error bar for the data points in Fig. 6(b) has a range from 0.0373 to 2.30 and the average standard deviation is 0.715, which is smaller than the symbol in the figure and thus is not shown.

Fig. 7 showed the degradation result for Methyl Orange by the SiO_2-Co core-shell nanoparticles at pH 3, showing a 96.7% degradation within one minute, which is better than the hollow Co nanoparticles by Sha's work (90%) [2] and zero-valent iron particles by Shih's work (95%) [55]. The reaction time needed for dye gradation from the SiO_2-Co core-shell nanoparticles is also faster than these of the hollow Co nanoparticles and zero-valent iron particles.

The above results indicate that faster Methyl Orange degradation rates can be achieved using core-shell structures with higher Co concentration. Varying Co^{2+} precursor concentration alters the surface structure of SiO_2-Co core-shell nanoparticles. In our case, the surface structure of metal Co shell changed with increasing Co concentration, which also increased the reaction rate. Kinetic studies revealed that Methyl Orange degradation by SiO_2-Co core-shell nanoparticles appeared to be first-order.

Regression analysis was performed on the degradation data. The regression model used is similar to the one proposed in the literature: [23,39]

$$C(t) = C_{final} + (C_o - C_{final}) \times e^{(-kt)} \quad (2)$$

$$\text{or} \quad \frac{C(t)}{C_o} = \frac{C_{final}}{C_o} + \left(1 - \frac{C_{final}}{C_o}\right) \times e^{(-kt)} \quad (3)$$

According to the Beer's law, absorption is proportional to concentration of the measured solution. Thus, Eqs. (2) and (3) can be written as:

$$A(t) = A_{final} + (A_o - A_{final}) \times e^{(-kt)} \quad (4)$$

$$\text{or} \quad \frac{A(t)}{A_o} = \frac{A_{final}}{A_o} + \left(1 - \frac{A_{final}}{A_o}\right) \times e^{(-kt)} \quad (5)$$

where C_{final} is the ultimate residual dye concentration, C_o represents the initial dye concentration, k represents the empirical rate constant (min^{-1}), A_0 represents the initial absorbance intensity and A represents the absorbance intensity.

The regression results are presented in Table S1 in Supplementary Material. Regression results for Methyl Orange degradation (25 mg/L, pH 2.5) by SiO_2-Co core-shell nanoparticles (50 mg) with

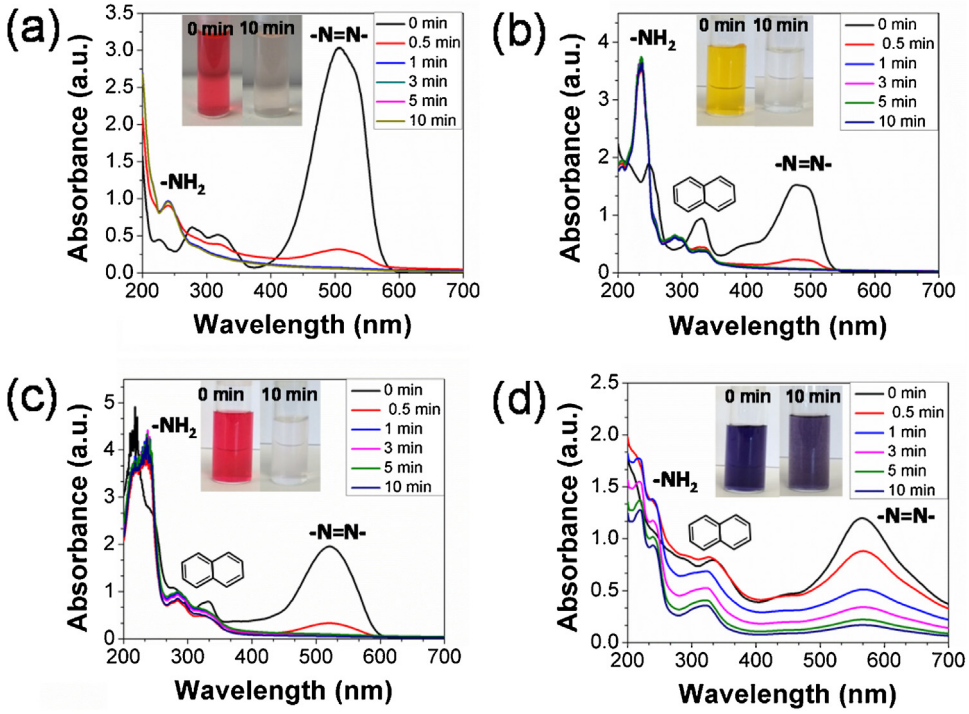

Fig. 8. UV/Vis absorption spectra of time dependent azo dye degradation by SiO_2-Co core-shell nanoparticles (CS-3) in the acidic environment (pH 2.5) and initial dye concentration of 0.076 mM (a) Methyl Orange; (b) Orange G; (c) Amaranth; (d) Congo Red. (For interpretation of the references to colour in the text, the reader is referred to the web version of this article.)

different Co shell structures showed that the correlation coefficients (R^2) are all over 0.96 which indicated that the data fit well with first order exponential decay kinetics, in agreement with other studies reported in the literature [39,55]. At pH 2.5, using hollow cobalt nanoparticles [2], Sha achieved a rate constant k of 2.444 min^{-1} and degradation efficiency of 99% within 4 min at an initial Methyl Orange concentration of 100 mg/L and hollow Co nanoparticle dosage of 0.5 g/L. At mild degradation conditions of pH 4, rate constant of 1.37 min^{-1} and efficiency of 66% were obtained within 10 min. At same condition of pH 2.5, k constant for our SiO_2-Co core-shell nanoparticles CS-3 is 4.84 min^{-1} and for SiO_2-Co core-shell nanoparticles CS-4 is 69.5 min^{-1}, much larger than Sha's results using hollow Co nanoparticles. Compared with Shih's work [55], the degradation rate constant is 1.1 min^{-1} at pH 3.1, which is smaller than our SiO_2-Co core-shell nanoparticles (CS-3) which has a rate constant of 3.83 min^{-1}.

3.5. SiO_2-Co nanoparticles for other azo dye degradation

The dye degradation experiment for three other different azo dyes, Orange G, Amaranth and Congo Red, were conducted and compared to Methyl Orange by adding 50 mg SiO_2-Co core-shell nanoparticles into each 40 ml dye solution (equivalent to 0.076 mM) at pH = 2.5. The time-dependent UV/Vis absorption measurement and their photographs before and after core-shell nanoparticle treatments were shown in Fig. 8. The colored dye solutions containing Methyl Orange, Orange G and Amaranth turned to clear after the core-shell nanoparticle treatment; all the three dyes contain only one azo group (—N=N—). However, the dye solution containing Congo Red only partially faded, which has two azo groups and is more complex than the other three dyes (molecular structures shown in Fig. S1).

Since the detailed discussion for Methyl Orange degradation has been described in Fig. 6 (a), the degradation of three other dyes, Orange G, Amaranth and Congo Red will be discussed below. As shown in Fig. 8(b), the UV/Vis spectra of Orange G showed the main characteristic absorption peak at 475 nm, which decreased over reaction time, indicating the degradation of the dye. At the same time, three new peaks appeared at 237 nm, 289 nm and 328 nm. The absorption peaks at 237 nm and 289 nm can be related to aniline, [56,57] one of the possible products of Orange G degradation, which contains an amine group and a benzene ring. The peak around 328 nm represents the group of naphthalene, which indicates another possible product of Orange G degradation, if the azo group broke in the middle of the dye. After 1 min reaction with the core-shell nanoparticles, 96.34% of Orange G solution faded into transparent solution, which indicates almost complete degradation, similar to the behavior of Methyl Orange degradation.

Fig. 8(c) showed the UV/Vis absorption spectra of Amaranth degradation as a function of reaction time; the absorption peaks for possible new products after degradation are out of data range of UV/Vis spectrometer and some noise was observed at low wavelength. In order to accurately identify the location for new peaks, a new experiment with a diluted solution of Amaranth (0.04 mM) was conducted while keeping the other conditions the same, and the results are shown in Fig. S6. Similar to Methyl Orange and Orange G, Amaranth is characterized by one main band with its maximum absorption at 521 nm, which decreased over the reaction time. It is observed that new peaks formed and increased at 224 nm, 242 nm, 285 nm and 320 nm. One of the possible products for Amaranth degradation by the core-shell nanoparticles is Naphthionic acid, which has been reported to have a broad absorption peak in the range of 270 nm–290 nm and can be used to explain the peak at 285 nm in our experiments [58]. The new peak at 242 nm is considered as the amine group (—NH_2). If the azo bond breaks, two possible products can be formed and both of them are biphenyl structures which may contribute to the new peak at 320 nm. All these new peaks indicate the cleavage of azo bond in Amaranth and new product formation.

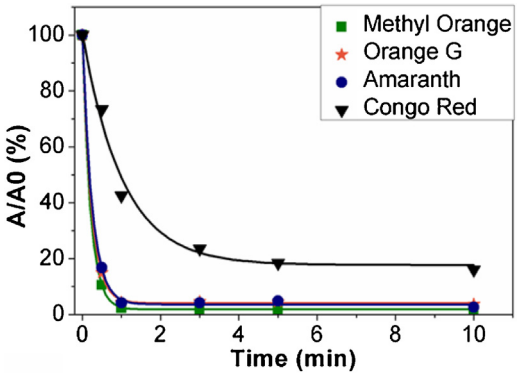

Fig. 9. Degradation kinetics of Methyl Orange, Congo Red, Amaranth and Orange G by SiO_2-Co nanoparticles (CS-3) in acidic environment (pH 2.5) and initial dye concentration of 0.076 mM.

In Fig. 8(d), Congo Red shows the characteristic absorption peak (—N=N—) at 565 nm and partial degradation as a function of reaction time. Even after 10 mins, the color of the Congo Red solution still not completely disappeared, indicating some dyes still exist. It is found that 86.01% of Congo Red were degraded which is much lower than the other three dyes. It is possible that the two azo groups in Congo Red require more core-shell nanoparticles involved in the reaction. Several new peaks were formed at 216 nm, 240 nm and 326 nm after the degradation. If both the "—N=N—" double bonds are broken, one of the possible products for Congo Red degradation is benzidine. Benzidine has UV/Vis absorption at wavelengths of 247 nm and 273 nm in acidic environment [59], which seems not completely matching with our new peaks. The peaks at 240 nm and 326 nm correspond to some amine group and naphthalene group, respectively. These results indicate that Congo Red degradation by the core-shell nanoparticles may not be similar to the other three dyes (Methyl Orange, Orange G and Amaranth) which only have one azo group. The two azo groups may have complicated the overall reaction. Some further degradation may have occurred, besides simple (—N=N—) bond breakage, which may lead to some other structures such as benzene ring structures. More investigation, with instruments such as gas chromatography mass spectrometry (GC–MS), or high performance liquid chromatography (HPLC)-MS is needed to further probe and confirm possible products for Congo Red degradation.

As shown in Fig. 9, at the same dosage of SiO_2-Co core-shell nanoparticles, when Methyl Orange, Orange G and Amaranth reached over 95% degradation, only about 86% Congo Red was degraded, due to the insufficiency of catalyst to cleave the second azo bond. Since the Congo Red contains two "—N=N—" groups, more SiO_2-Co core-shell nanoparticles were needed for complete degradation. To prove that the SiO_2-Co core-shell nanoparticles can effectively and completely degrade Congo Red, the concentration of Congo Red was decreased by half, while keeping the same catalyst amount. As shown in Fig. S7, the initial UV/Vis absorption peak for Congo Red was seen at 565 nm. When 50 mg SiO_2-Co core-shell nanoparticles were added to 40 ml dye solution (0.04 mM), solution color changed to colorless within 1 min at room temperature, with new peaks formed concurrently at 216 nm, 240 nm and 326 nm wavelengths, which confirmed the breakage of azo group and new product formation, with near complete breakage of both "—N=N—" double bonds in the dye structure.

Same as Methyl Orange degradation, the kinetic constants A_0, A_{final} and k for Orange G, Amaranth and Congo Red degradation were obtained by exponential regression from the experimental data. The regression results are presented in Table S2 in Supplementary Material. Regression results for azo dye degradation by SiO_2-Co core-shell nanoparticles (CS-3) showed that the experimental data fit well with first order exponential decay kinetics. For Methyl Orange, Orange G and Amaranth, there is only one "—N=N—" bond. The k constants are 5.44 min^{-1}, 6.59 min^{-1}, and 5.60 min^{-1} for Methyl Orange, Orange G, and Amaranth, respectively; only small difference can be found among these three dyes. As Congo Red has two "—N=N—" bonds, degradation rate is much slower, and the k constant is only 0.98 min^{-1} under similar reaction conditions.

4. Conclusions

SiO_2-Co core-shell nanoparticles sizes around 75 nm were successfully synthesized using a multi-step method at ambient conditions. SiO_2 nanoparticle synthesis based on Stöber method is highly related to the ratio of reactant, especially the concentration of catalyst ammonia and reaction time. The resulting 50 nm SiO_2 nanoparticles were then surface modified by APTES for use in subsequent core-shell nanoparticle fabrication. APTES concentration of 5 mM gives the best siloxane surface modification on SiO_2 nanoparticles. These SiO_2-Co core-shell nanoparticles proved efficient for the reductive degradation of a wide range of azo dyes, including Methyl Orange, Congo Red, Amaranth, and Orange G. The reaction kinetics appeared to be first order and the fastest reaction constant achieved was 69.5 min^{-1} for Methyl Orange degradation at a pH value of 2.5. UV/Vis measurements indicated new reaction products formation and successful cleavage of the "—N=N—" bonds in the azo dyes, showing reductive degradation instead of simple decolorization.

Acknowledgements

Financial support from MicroChem Corp is greatly acknowledged.

Appendix A. Supplementary data

Supplementary data associated with this article can be found, in the online version, at http://dx.doi.org/10.1016/j.apcatb.2016.06.030.

References

[1] Y.L. Pang, A.Z. Abdullah, Current status of textile industry wastewater management and research progress in Malaysia: a review, CLEAN—Soil, Air, Water 41 (8) (2013) 751–764.
[2] Y. Sha, I. Mathew, Q. Cui, M. Clay, F. Gao, X. Zhang, Z. Gu, Rapid degradation of azo dye methyl orange using hollow cobalt nanoparticles, Chemosphere 144 (2016) 1530–1535.
[3] V. Meshko, L. Markovska, M. Mincheva, A.E. Rodrigues, Adsorption of basic dyes on granular acivated carbon and natural zeolite, Water Res. 35 (14) (2001) 3357–3366.
[4] J. Ma, F. Yu, L. Zhou, L. jin, M. Yang, J. Luan, Y. Tang, H. Fan, Z. Yuan, J. Chen, Enhanced adsorptive removal of methyl orange and methylene blue from aqueous solution by alkali-activated multiwalled carbon nanotubes, ACS Appl. Mater. Interfaces 4 (11) (2012) 5749–5760.
[5] L. Wang, X.L. Wu, W.H. Xu, X.J. Huang, J.H. Liu, A.W. Xu, Stable organic–inorganic hybrid of polyaniline/α-zirconium phosphate for efficient removal of organic pollutants in water environment, ACS Appl. Mater. Interfaces 4 (5) (2012) 2686–2692.
[6] A. Meng, J. Xing, Z. Li, Q. Li, Cr-doped ZnO nanoparticles: synthesis, characterization, adsorption property, and recyclability, ACS Appl. Mater. Interfaces 7 (49) (2015) 27449–27457.
[7] A.B. dos Santos, F.J. Cervantes, J.B. van Lier, Review paper on current technologies for decolourisation of textile wastewaters: perspectives for anaerobic biotechnology, Bioresour. Technol. 98 (12) (2007) 2369–2385.
[8] T. Robinson, G. McMullan, R. Marchant, P. Nigam, Remediation of dyes in textile effluent: a critical review on current treatment technologies with a proposed alternative, Bioresour. Technol. 77 (3) (2001) 247–255.
[9] J. Labanda, J. Sabaté, J. Llorens, Modeling of the dynamic adsorption of an anionic dye through ion-exchange membrane adsorber, J. Membr. Sci. 340 (1) (2009) 234–240.
[10] J.-S. Wu, C.H. Liu, K.H. Chu, S.Y. Suen, Removal of cationic dye methyl violet 2B from water by cation exchange membranes, J. Membr. Sci. 309 (1) (2008) 239–245.

[11] D. Wesenberg, I. Kyriakides, S.N. Agathos, White-rot fungi and their enzymes for the treatment of industrial dye effluents, Biotechnol. Adv. 22 (1) (2003) 161–187.
[12] A. Paszczynski, R.L. Crawford, Degradation of azo compounds by ligninase from Phanerochaete chrysosporium: involvement of veratryl alcohol, Biochem. Biophys. Res. Commun. 178 (3) (1991) 1056–1063.
[13] A. Paszczynski, M.B. Pasti, S. Goszczynski, D.L. Crawford, R.L. Crawford, New approach to improve degradation of recalcitrant azo dyes by Streptomyces spp. and Phanerochaete chrysosporium, Enzyme Microb. Technol. 13 (5) (1991) 378–384.
[14] M.A. Martins, M.H. Cardoso, M.J. Queiroz, M.T. Ramalho, A.M. Campos, Biodegradation of azo dyes by the yeast Candida zeylanoides in batch aerated cultures, Chemosphere 38 (11) (1999) 2455–2460.
[15] N. Kirby, R. Marchant, G. McMullan, Decolourisation of synthetic textile dyes by Phlebia tremellosa, FEMS Microbiol. Lett. 188 (1) (2000) 93–96.
[16] R. Gingell, R. Walker, Mechanisms of azo reduction by Streptococcus faecalis II. The role of soluble flavins, Xenobiotica 1 (3) (1971) 231–239.
[17] I.M. Banat, P. Nigam, D. Singh, R. Marchant, Microbial decolorization of textile-dyecontaining effluents: a review, Bioresour. Technol. 58 (3) (1996) 217–227.
[18] A.T. Moore, A. Vira, S. Fogel, Biodegradation of trans-1, 2-dichloroethylene by methane-utilizing bacteria in an aquifer simulator, Environ. Sci. Technol. 23 (4) (1989) 403–406.
[19] I. Arslan, I.A. Balcioğlu, Degradation of commercial reactive dyestuffs by heterogenous and homogenous advanced oxidation processes: a comparative study, Dyes Pigment. 43 (2) (1999) 95–108.
[20] P. Cooper, Removing colour from dyehouse waste waters—a critical review of technology available, J. Soc. Dyers Colour. 109 (3) (1993) 97–100.
[21] U. Pagga, K. Taeger, Development of a method for adsorption of dyestuffs on activated sludge, Water Res. 28 (5) (1994) 1051–1057.
[22] A. Houas, H. Lachheb, M. Ksibi, E. Elaloui, C. Guillard, J.M. Herrmann, Photocatalytic degradation pathway of methylene blue in water, Appl. Catal. B: Environ. 31 (2) (2001) 145–157.
[23] H.-Y. Shu, M.C. Chang, H.H. Yu, W.H. Chen, Reduction of an azo dye acid black 24 solution using synthesized nanoscale zerovalent iron particles, J. Colloid Interface Sci. 314 (1) (2007) 89–97.
[24] C. Galindo, P. Jacques, A. Kalt, Photooxidation of the phenylazonaphthol AO_{20} on TiO_2: kinetic and mechanistic investigations, Chemosphere 45 (6) (2001) 997–1005.
[25] W.Z. Tang, H. An, UV/TiO_2 photocatalytic oxidation of commercial dyes in aqueous solutions, Chemosphere 31 (9) (1995) 4157–4170.
[26] E. Forgacs, T. Cserhati, G. Oros, Removal of synthetic dyes from wastewaters: a review, Environ. Int. 30 (7) (2004) 953–971.
[27] Y. Anjaneyulu, N.S. Chary, D.S.S. Raj, Decolourization of industrial effluents–available methods and emerging technologies–a review, Rev. Environ. Sci. Bio/Technol. 4 (4) (2005) 245–273.
[28] P.C. Vandevivere, R. Bianchi, W. Verstraete, Review: treatment and reuse of wastewater from the textile wet-processing industry: review of emerging technologies, J. Chem. Technol. Biotechnol. (72) (1999) 289–302.
[29] R.-C. Wang, K.-S. Fan, J.-S. Chang, Removal of acid dye by ZnFe 2 O 4/TiO 2-immobilized granular activated carbon under visible light irradiation in a recycle liquid–solid fluidized bed, J. Taiwan Inst. Chem. Eng. 40 (5) (2009) 533–540.
[30] C. Jiang, Z. Gao, H. Qu, J. Li, X. Wang, P. Li, H. Liu, A new insight into Fenton and Fenton-like processes for water treatment: part II. Influence of organic compounds on Fe (III)/Fe (II) interconversion and the course of reactions, J. Hazard. Mater. 250 (2013) 76–81.
[31] J. Liao, S. Lin, L. Zhang, N. Pan, X. Cao, J. Li, Photocatalytic degradation of methyl orange using a TiO2/Ti mesh electrode with 3D nanotube arrays, ACS Appl. Mater. Interfaces 4 (1) (2011) 171–177.
[32] Y. Yang, G. Wang, Q. Deng, D.H.L. Ng, H. Zhao, Microwave-assisted fabrication of nanoparticulate TiO2 microspheres for synergistic photocatalytic removal of Cr (VI) and methyl orange, ACS Appl. Mater. Interfaces 6 (4) (2014) 3008–3015.
[33] W.S. Pereira, R.S. Freire, Azo dye degradation by recycled waste zero-valent iron powder, J. Braz. Chem. Soc. 17 (5) (2006) 832–838.
[34] J. Cao, L. Wei, Q. Huang, L. Wang, S. Han, Reducing degradation of azo dye by zero-valent iron in aqueous solution, Chemosphere 38 (3) (1999) 565–571.
[35] P. Liu, J.L. Zhang, M.Q. Zha, C.H. Shek, Synthesis of an Fe rich amorphous structure with a catalytic effect to rapidly decolorize azo dye at room temperature, ACS Appl. Mater. Interfaces 6 (8) (2014) 5500–5505.
[36] S. Rodriguez, L. Vasquez, A. Romero, A. Santos, Dye oxidation in aqueous phase by using zero-Valent iron as persulfate activator: kinetic model and effect of particle size, Ind. Eng. Chem. Res. 53 (31) (2014) 12288–12294.
[37] A.D. Bokare, R.C. Chikate, C.V. Rode, K.M. Paknikar, Iron-nickel bimetallic nanoparticles for reductive degradation of azo dye Orange G in aqueous solution, Appl. Catal. B: Environ. 79 (3) (2008) 270–278.
[38] M. Mohl, A. Kumar, A.L.M. Reddy, A. Kukovecz, A. Konya, I. Kiricsi, R. Vajtai, P.M. Ajayan, Synthesis of catalytic porous metallic nanorods by galvanic exchange reaction, J. Phys. Chem. C 114 (1) (2009) 389–393.
[39] J. Fan, Y. Guo, J. Wang, M. Fan, Rapid decolorization of azo dye methyl orange in aqueous solution by nanoscale zerovalent iron particles, J. Hazard. Mater. 166 (2) (2009) 904–910.
[40] V. Balzani, Nanoscience and nanotechnology: the bottom-up construction of molecular devices and machines, Pure Appl. Chem. 80 (8) (2008) 1631–1650.
[41] M. Alejandro-Arellano, et al., Silica-coated metals and semiconductors. Stabilization and nanostructuring, Pure Appl. Chem. 72 (1–2) (2000) 257–267.
[42] M.A. Correa-Duarte, M. Giersig, L.M. Liz-Marzan, Stabilization of CdS semiconductor nanoparticles against photodegradation by a silica coating procedure, Chem. Phys. Lett. 286 (5) (1998) 497–501.
[43] J. Smith, J. Meadows, P. Williams, Adsorption of polyvinylpyrrolidone onto polystyrene latices and the effect on colloid stability, Langmuir 12 (16) (1996) 3773–3778.
[44] W. Stöber, A. Fink, E. Bohn, Controlled growth of monodisperse silica spheres in the micron size range, J. Colloid Interface Sci. 26 (1) (1968) 62–69.
[45] X.-D. Wang, Z.X. Shen, T. Sang, X.B. Cheng, M.F. Li, L.Y. Chen, Z.S. Wang, Preparation of spherical silica particles by Stöber process with high concentration of tetra-ethyl-orthosilicate, J. Colloid Interface Sci. 341 (1) (2010) 23–29.
[46] L. Zhuravlev, The surface chemistry of amorphous silica. Zhuravlev model, Colloids Surf. A: Physicochem. Eng. Aspects 173 (1) (2000) 1–38.
[47] T. Luts, W. Suprun, D. Hofmann, O. Klepel, H. Papp, Epoxidation of olefins catalyzed by novel Mn (III) and Mo (IV) salen complexes immobilized on mesoporous silica gel: part I. Synthesis and characterization of homogeneous and immobilized Mn (III) and Mo (IV) Salen complexes, J. Mol. Catal. A: Chem. 261 (1) (2007) 16–23.
[48] R. Bai, X. Fu, H. Bao, W. Ren, Chiral Salen Mn (III) complex axial coordination immobilized on diamine modified ZSPP and their catalytic epoxidation of styrene, Catal. Commun. 9 (7) (2008) 1588–1594.
[49] V. Salgueiriño-Maceira, M.A. Correa-Duarte, Cobalt and silica based core–shell structured nanospheres, J. Mater. Chem. 16 (36) (2006) 3593–3597.
[50] V. Salgueirino-Maceira, et al., Synthesis and characterization of large colloidal cobalt particles, Langmuir 22 (4) (2006) 1455–1458.
[51] J. Ahmed, T. Ahmad, K.V. Ramanujachary, S.E. Lofland, A.K. Ganguli, Development of a microemulsion-based process for synthesis of cobalt (Co) and cobalt oxide (Co_3O_4) nanoparticles from submicrometer rods of cobalt oxalate, J. Colloid Interface Sci. 321 (2) (2008) 434–441.
[52] N.M. Aljamali, Review in azo compounds and its biological activity, Biochem. Anal. Biochem. (2015) (2015).
[53] C. Galindo, P. Jacques, A. Kalt, Photodegradation of the aminoazobenzene acid orange 52 by three advanced oxidation processes: UV/H_2O_2, UV/TiO_2 and VIS/TiO_2: comparative mechanistic and kinetic investigations, J. Photochem. Photobiol. A: Chem. 130 (1) (2000) 35–47.
[54] J. Gu, S. Kan, Q. Shen, J. Kan, Effects of sulfanilic acid and anthranilic acid on electrochemical stability of polyaniline, Int. J. Electrochem. Sci. 9 (2014) 6858–6869.
[55] Y.-H. Shih, C.-P. Tso, L.-Y. Tung, Rapid degradation of methyl orange with nanoscale zerovalent iron particles, Nanotechnology 7 (2010) 16–17.
[56] T.C.S. Lin, W.C. Lin, Ultra-violet absorption spectra of aniline, β-naphthylamine and β-naphthol, J. Chin. Chem. Soc. 8 (3) (1961) 156–164.
[57] S. Kumar, Organic Chemistry: Spectroscopy of Organic Compounds, Guru Nanak Dev University, Amritsar, 2006, pp. 1–17.
[58] M.H. Mohamed, L.D. Wilson, J.V. Headley, K.M. Peru, Screening of oil sands naphthenic acids by UV–vis absorption and fluorescence emission spectrophotometry, J. Environ. Sci. Health Part A 43 (14) (2008) 1700–1705.
[59] G. Reartes, S. Liberman, M. Blesa, Acidity constants of benzidine in aqueous solutions, Talanta 34 (12) (1987) 1039–1042.